

Supplementary Information

Ambipolar, low-voltage, and low-hysteresis PbSe nanowire field-effect transistors by electrolyte gating

Irina Lokteva, Stefan Thiemann, Florentina Gannott and Jana Zaumseil*

Institute of Polymer Materials, Friedrich-Alexander Universität Erlangen-Nürnberg, Martensstraße 7, D-91058 Erlangen, Germany. E-mail: jana.zaumseil@ww.uni-erlangen.de

Figure S1: Diameter distribution of PbSe NWs

Figure S2: Transfer characteristics of the electrolyte-gated FET showing negligible gate leakage

Figure S3: Transfer characteristics of the electrolyte-gated device *versus* gate and reference voltage

Figure S4: Linear electron and hole mobilities for a Si/SiO₂ and electrolyte-gated PbSe NW-FET

Figure S5: Transfer characteristics of an electrolyte-gated FET and corresponding mobilities calculated with constant specific capacitance $C_i = 3.4 \mu\text{F}/\text{cm}^2$

Figure S6: Voltage-dependent capacitance of PbSe NWs/[EMIM][FAP] interface by impedance measurements and corresponding mobilities

Figure S7: Dynamic gate-displacement current measurements of an electrolyte-gated FET with corresponding gate-dependent capacitances and extracted mobilities

Figure S8: Transfer characteristics of an electrolyte-gated device before and after hydrazine treatment

Figure S9: FTIR spectra of the PbSe NWs before and after hydrazine treatment

Figure S10: Output characteristics of an ion gel-gated FET

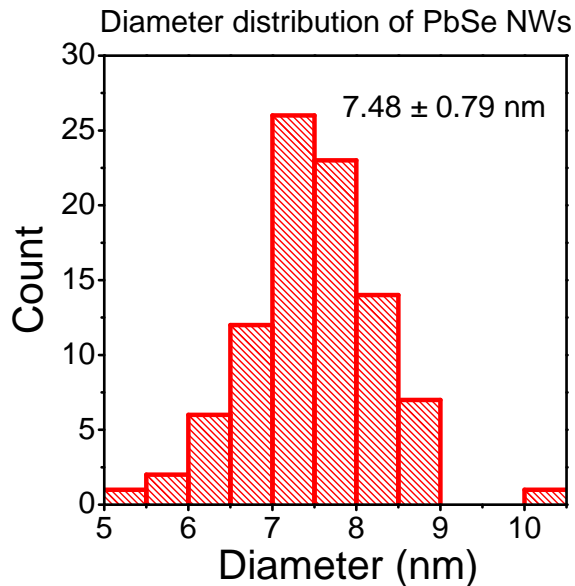


Figure S1 Diameter distribution of as-synthesized PbSe NWs as determined by TEM.

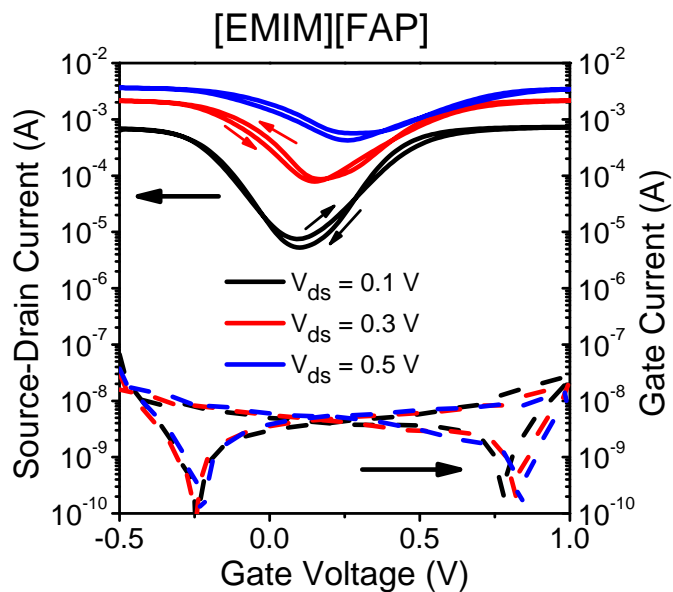


Figure S2 Transfer characteristics of the electrolyte-gated PbSe NW-FET in Fig. 2B showing negligible gate current leakage ($L = 10 \mu\text{m}$).

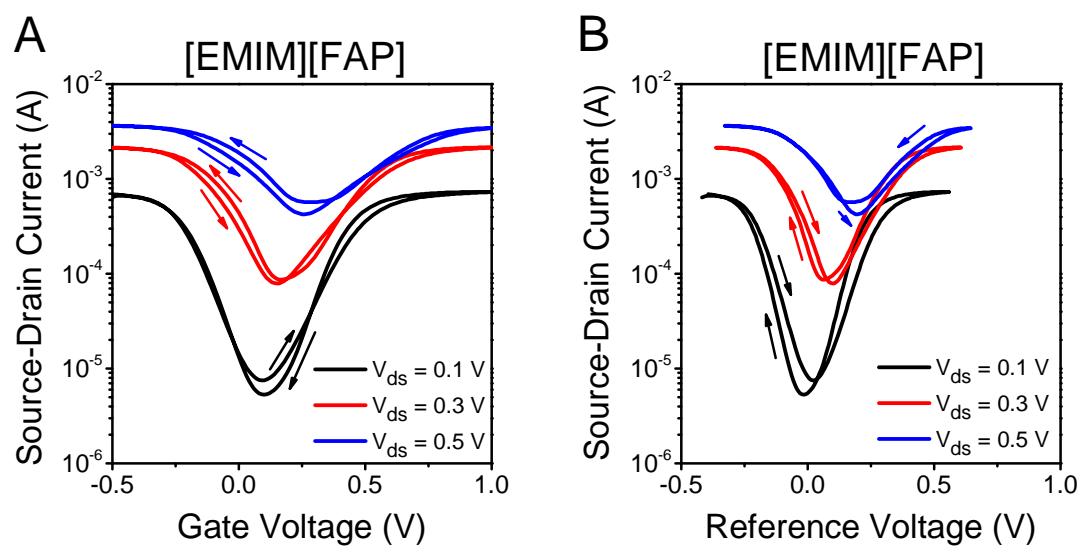


Figure S3 Transfer characteristics of the electrolyte-gated PbSe NW-FET in Fig. 2B *versus* the applied gate voltage (A) and referenced against an oxidized silver electrode (B) ($L = 10 \mu\text{m}$).

Mobility calculations

The apparent field-effect mobilities of the PbSe NW-FETs were calculated from the transconductance in the linear regime at $V_{ds} = 0.01$ V for electrons and -0.01 V for holes, taking into account only the channel geometry and not the number of nanowires as follows:

$$\mu_{lin} = \frac{\partial I_{ds}}{\partial V_g} \cdot \frac{L}{WC_i V_{ds}} \quad (1)$$

where C_i is the capacitance per unit area of the gate dielectric (11.5 nF/cm² for 300 nm of SiO₂ and 3.4 μF/cm² for [EMIM][FAP], estimated from impedance measurements (LCR-bridge, C_p -mode) on a Pt/ionic liquid/Pt sandwich structure. The mobilities represented in Figures S4 and S5 were calculated according to equation (1).

Additionally, we measured the voltage dependent capacitance of the ionic liquid/PbSe NWs interface in a typical PbSe NW-FET using an LCR-meter in C_p -mode at a constant frequency of 20 Hz. The specific capacitance of ionic liquids depends on the applied AC-frequency during impedance measurements, due to the movement of the ions and increases with decreasing frequency. However, at frequencies below 100 Hz the capacitance reaches a plateau and does not increase further as shown for [EMIM][FAP] by Thiemann et al. (Ref. 22). The lowest possible frequency of the LCR meter 4980A (20 Hz) can thus be used to determine the quasi-static capacitance necessary for the mobility calculations. The source and drain electrodes were shorted and connected to the low input and the gate electrode (platinum wire) was connected to the high input. Due to the structure of our device, which exposes not only the channel but also the electrodes to the ionic liquid (*i.e.*, acting as an additional capacitor in parallel), the capacitance C of the active channel region was determined as the difference between the capacitance of the device with NWs and identical electrodes without NWs. The gate voltage was swept from 0 to 1 V for electrons and 0 to -1 V for holes. C_i in equation (1) can be substituted by $C_i = C/(W \cdot L)$ giving:

$$\mu_{lin} = \frac{\partial I_{ds}}{\partial V_g} \cdot \frac{L^2}{CV_{ds}} \quad (2)$$

We can thus determine the gate voltage dependent mobility for this device without knowing of the exact channel width, *i.e.*, the number of nanowires in the channel. Figure S6 shows the extracted voltage dependent capacitances and hole and electron mobilities.

Additionally, the gate-dependent capacitance values were estimated from displacement current measurements at the sweep rates of 1.10 , 1.58 , 2.98 and 4.24 V/s. In these measurements, the source/drain contacts were grounded and the displacement current due the PbSe NWs with [EMIM][FAP] was determined as the difference between currents obtained for two identical devices with and without NWs under the same conditions. The gate voltages were swept from 0 to 1 V for electrons and 0 to -1 V for holes. The gate voltage dependent capacitances for electrons and holes were calculated as follows:

$$C = \frac{I_{disp}}{r_v} \quad (3)$$

where r_v is the scan rate in V/s. These capacitance values were applied in equation (2) to extract gate voltage dependent mobilities, which are shown in Figure S7. Note that due to the ambipolar nature of the devices without a well-defined off state the estimation of injected charges is rather difficult compared to unipolar devices and the margins of error might be quite high.

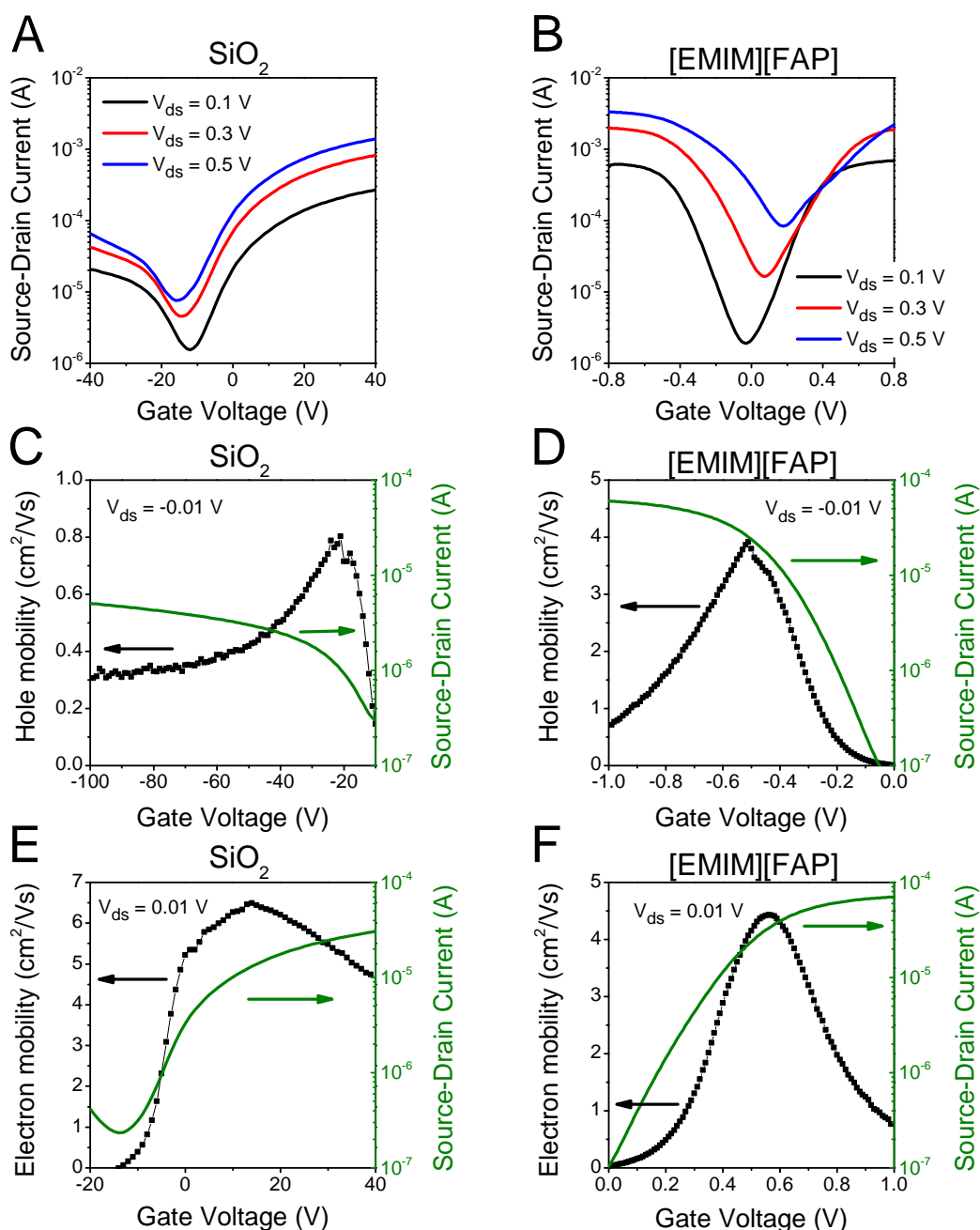


Figure S4 Comparison of mobilities of the back-gated and electrolyte-gated PbSe NW FET. Transfer characteristics of a typical PbSe NW-FET with channel length of $20 \mu\text{m}$ with (A) back-gating and (B) electrolyte-gating. Apparent linear field-effect mobilities of this FET calculated using equation (1): (C) and (F) hole and electron mobilities of the back-gated device with $V_{ds} = -0.01 \text{ V}$ and 0.01 V , respectively; (D) and (F) hole and electron mobilities of the electrolyte-gated device with $V_{ds} = -0.01 \text{ V}$ and 0.01 V , respectively, using a constant capacitance of $C_i = 3.4 \mu\text{F}/\text{cm}^2$ for equation (1).

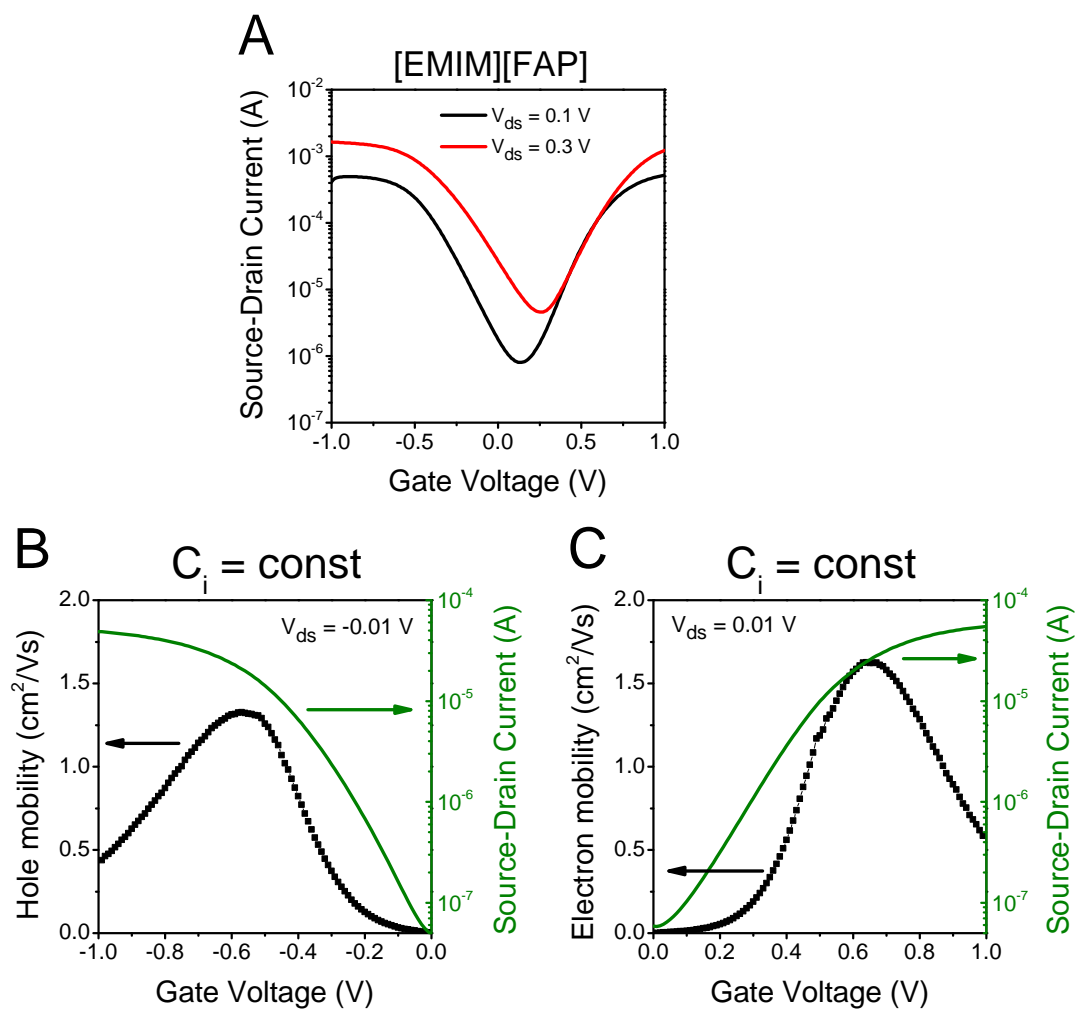


Figure S5 (A) Transfer characteristics of a typical electrolyte-gated PbSe NW-FET with channel length of $10 \mu\text{m}$. (B) and (C) apparent linear hole and electron field-effect mobilities calculated from transconductance using equation (1) with a constant specific capacitance $C_i = 3.4 \mu\text{F}/\text{cm}^2$.

C(V_g) Impedance measurements

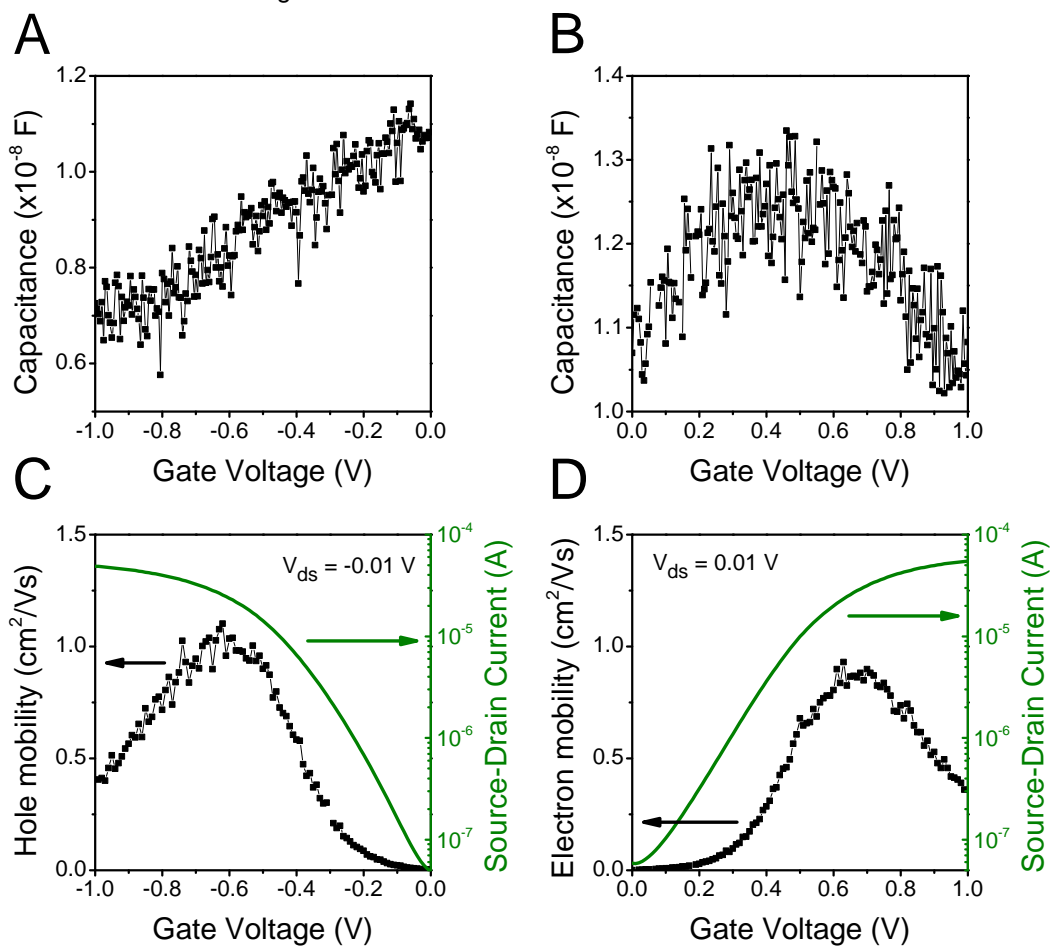


Figure S6 (A) and (B) Voltage-dependent capacitance of PbSe NWs/[EMIM][FAP] interface by impedance measurements (LCR-meter, C_p -mode, frequency 20 Hz) for the same electrolyte-gated device as shown in Figure S5 ($L = 10 \mu\text{m}$). (C) and (D) corresponding apparent linear hole and electron field-effect mobilities calculated from equation (2) with $V_{ds} = -0.01$ V and 0.01 V, respectively.

Displacement current measurements

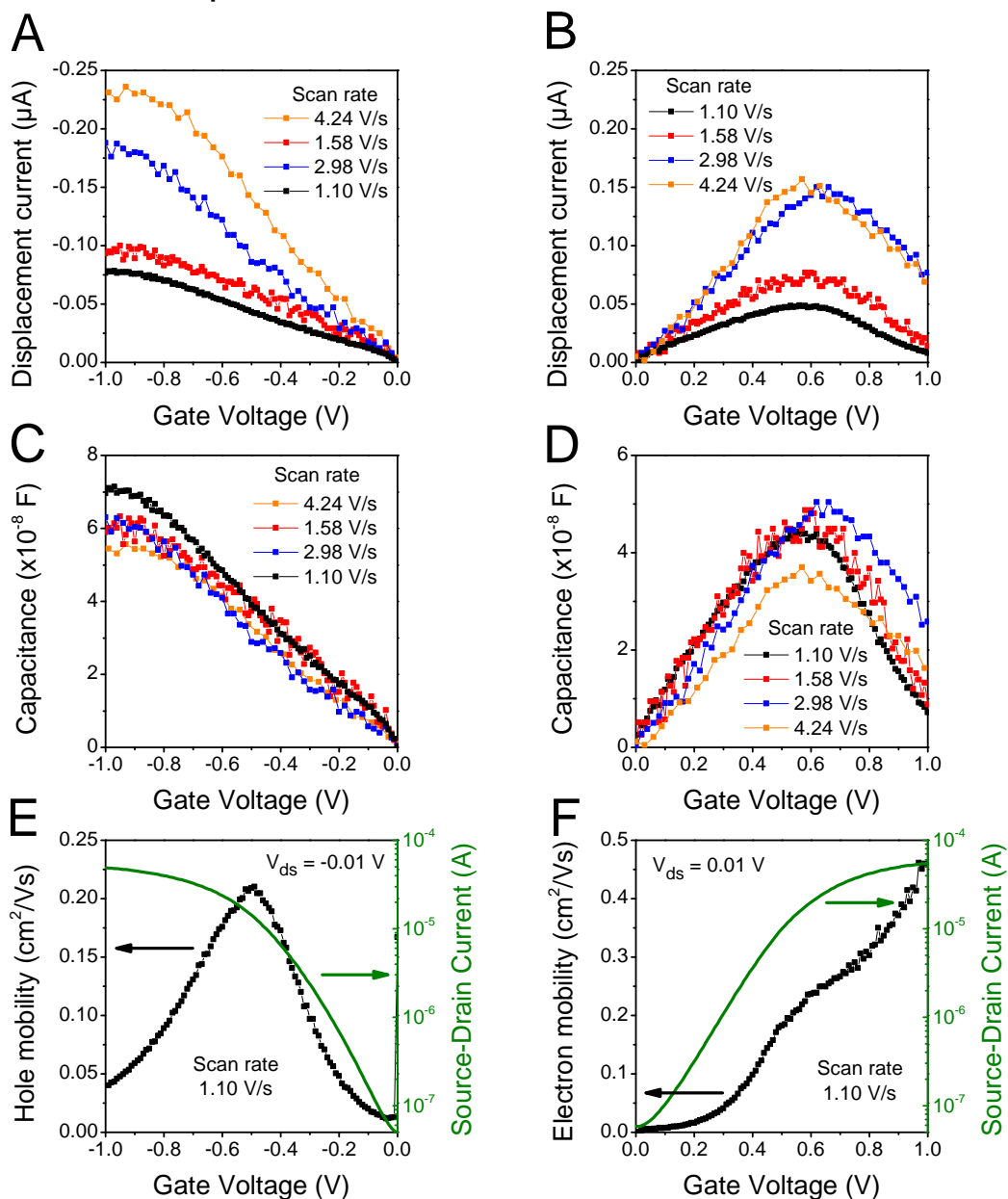


Figure S7 (A) and (B) Dynamic gate-displacement current measurements of the same electrolyte-gated device as shown in Figure S5 at various sweep rates at negative and positive gate voltages ($L = 10 \mu\text{m}$). (C) and (D) corresponding gate-dependent capacitances calculated with equation (3). (E) and (F) corresponding linear hole and electron field-effect mobilities.

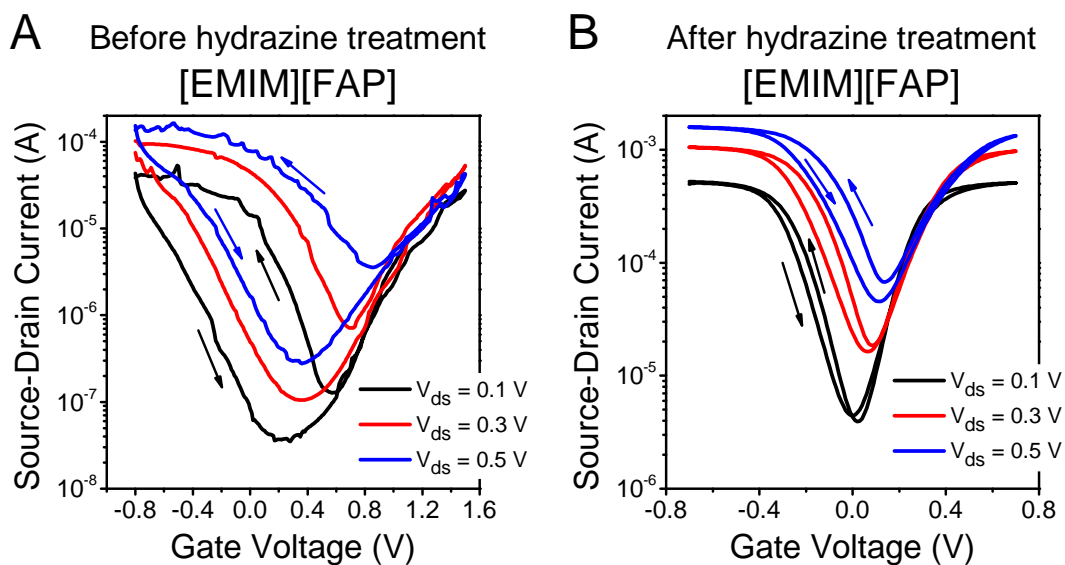


Figure S8 Transfer characteristics of an electrolyte-gated PbSe NW-FET ($L = 10 \mu\text{m}$) (A) before hydrazine treatment and (B) after 1 min exposure to a 1 molar hydrazine solution in tetrahydrofuran.

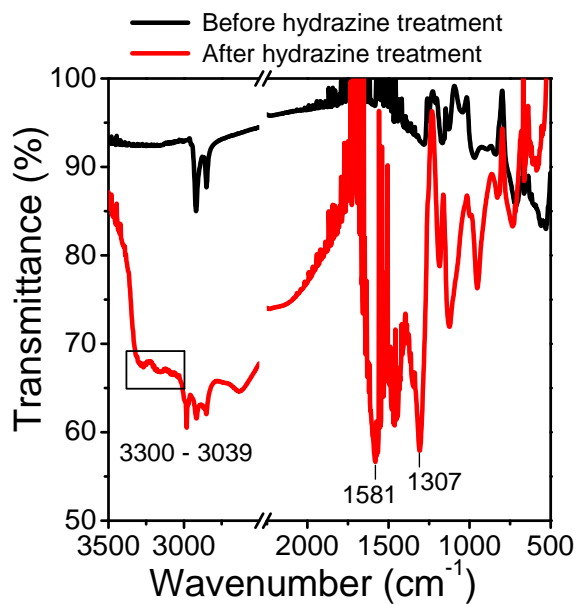


Figure S9 FTIR spectra of the PbSe NWs before and after hydrazine treatment (1 min exposure to a 1 molar hydrazine solution in tetrahydrofuran).

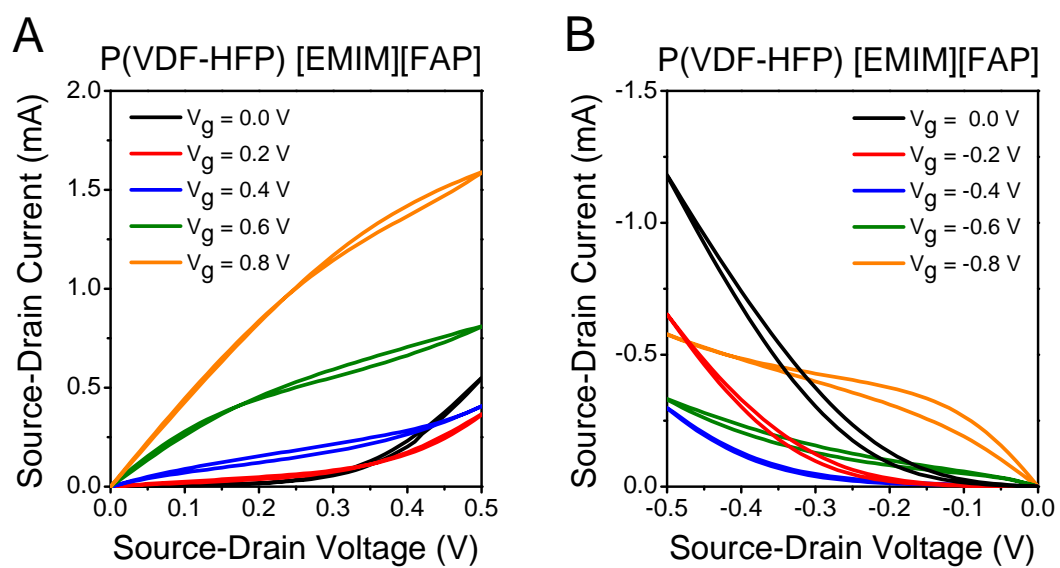


Figure S10 Output characteristics of an ion gel-gated PbSe NW-FET ($L = 5 \mu\text{m}$) at (A) positive and (B) negative source-drain voltages. The gate voltage was applied *via* a gold side gate electrode.